Journal of Cultural Heritage 15 (2014) 283–291

Available online at
SciVerse ScienceDirect
www.sciencedirect.com

Elsevier Masson France
EM|consulte
www.em-consulte.com/en

Original article

Chinese archaeological artefacts: Microstructure and corrosion behaviour of high-leaded bronzes

Marta Quaranta , Emilio Catelli , Silvia Prati , Giorgia Sciutto , Rocco Mazzeo*

University of Bologna, M2ADL – Microchemistry and Microscopy Art Diagnostic Laboratory, 42, Via Guaccimanni, 48100 Ravenna, Italy

ARTICLE INFO

Article history:
Received 15 February 2013
Accepted 10 July 2013
Available online 2 August 2013

Keywords:
High-leaded bronze
Lead globules corrosion
Scanning electron microscopy
μRaman spectroscopy
Pourbaix diagrams

ABSTRACT

Metallographic features of ancient bronze artefacts often hide peculiar micro-chemical processes and corrosion behaviours, which are worth to be studied as they can provide conservators and archaeologists with valuable tools and information. It is widely documented that Chinese bronzes were cast and the way to adjust their properties was to change the alloy composition. In particular, addition of lead, which is insoluble in the bronze matrix, results in the formation of inclusions or globules, which undergo oxidation processes leading to their conversion into corrosion products. The mechanisms through which this occurs were still poorly investigated. The present work was conducted to further study the corrosion behaviour of high-leaded bronze, especially focusing on the behaviour of lead globules. To this aim, a collection of Chinese archaeological bronzes, showing intermediate steps of degradation, were selected and investigated. The use of combined microscopy-based, molecular and elemental, analytical techniques allowed the characterization as well as the precise location of corrosion products, thus enabling us to propose a degradation pathway basing on thermodynamic data provided by Pourbaix diagram. The achieved results will be useful for researchers involved in these kinds of studies to better interpret data obtained.

© 2013 Elsevier Masson SAS. All rights reserved.

1. Research aims

The presented research provides an overview of corrosion behaviour of high-leaded bronze and peculiar features are highlighted. We introduce a state-of-the-art of knowledge concerning these issues, in order to interpret the obtained data in a wider perspective.

In the literature, it is well documented how these bronzes show lead inclusions of variable dimensions, whose origin was not still well understood. In particular, Chinese bronzes were produced using a high amount of lead, which is not soluble in the copper alloy and form inclusions of variable dimensions. They are found corroded in archeological finds sometimes transformed in copper-based corrosion products.

The aim of the study is to comprehend the mechanisms though which leads globule corrode into cuprite. It should be mentioned that long-term processes are hardly reproducible in laboratory experiments; empirical observation and development of phenomenological theories, relying on a large number of archaeological samples, represent the best approach to the problem, which could lead to the formulation of theories on degradation pathway.

Therefore, it is the authors' opinion, that an effective way to prove and validate hypothesis is to analyse archaeological samples exhibiting intermediate steps of degradation. The identification of intermediate stages of degradation has allowed us to propose a sequence leading to the overall substitution of the original lead globule into cuprite.

The results would be significant for archaeologists or conservation scientists who, examining high-leaded bronze artefacts, would face the occurrence of these corrosion behaviour.

2. Introduction

Metallographic features of ancient bronze artefacts often hide peculiar and specific corrosion behaviours, which are worth to be studied as they can provide conservators and archaeologists with valuable tools and information. These are useful to foresee an appropriate conservation treatment and to define proper exposure conditions, in order to reduce corrosion rates [1].

Bronze commonly refers to a copper-tin alloy, which can have a variable tin content and can also contain other alloying elements, such as lead, which is added on purpose, or minor elements, according to local copper ores [2–4].

Concerning Chinese bronzes, it is well known and documented that they were cast and the way to adjust their properties (hardness, ability to hold an edge, reflectance, sound for bells) was to change the alloy composition [5]. Addition of Pb (up to 50%, i.e.

* Corresponding author. Tel.: +390544937150; fax: +390544937159.
E-mail address: rocco.mazzeo@unibo.it (R. Mazzeo).

1296-2074/$ – see front matter © 2013 Elsevier Masson SAS. All rights reserved.
http://dx.doi.org/10.1016/j.culher.2013.07.007

Table 1
Uncommon inclusions (cuprite, lead and unalloyed copper, UCI) in bronzes described in the literature.

Artefact	Sn (%)	Pb (%)	Cuprite	Pb	UCI	Ref.
Chinese Bronze mirror with zodiacal animals (Sui dynasty, 600 B.C.)	24	Traces			Round structures where redeposited Cu is replacing cuprite formed in place of Pb globules; linear areas where redeposited copper is replacing cuprite in the outer layer of corrosion	[6,8]
Chinese bronze bell (tomb of the Marquis of Cai, Shou Xian, 450 BC)	Moderately high tin	Traces			Round structures where redeposited Cu is replacing cuprite formed in place of Pb globules; linear areas where redeposited copper is replacing cuprite in the outer layer of corrosion	[6,8]
Chinese Bronze Hu ceremonial vessel (Zhou Dynasty)	21.8	4.1			Irregular islands that replace Pb droplets in the corroded (α+δ) eutectoid	[7,8]
Solder lump on the handle of Chinese bronze Kuei ceremonial vessel	21	9			Globules that replace Pb droplets in the corroded (α+δ) eutectoid	[7,8]
Chinese Jin bronzes (vessel and horse fittings), Zhou dynasty	-	-			Interdendritic particles replacing eutectoid	[8,9]
Part of a vessel	20–22	4.1–4.6		Pb inclusions large and of irregular shape	As inclusion in Pb globules	[14]
Chinese money tree (*yaoquianshul*) from the Eastern Han dynasty	17	8	Cuprite globules that replace Pb in Pb droplets	Corroded lead droplets		[13]
Relics found in ancient burial pits in the Liangdai village, Shaanxi Province, Northwest	13.2–21.9	2.4–15.2	Cuprite globules mostly found where metal core is corroded, sometimes include Pb corrosion products	Pb globules partly corroded	Irregular inclusion that replace Pb droplets in the corroded (α+δ) eutectoid	The present study

coins) resulted in an improved fluidity and mould-filling capability (particularly the casting of finely detailed objects), while the addition of 5–15% tin produced a harder bronze alloy, which melted at a lower temperature [5]. The presence of lead does not affect the structures after solidification as it does not go into solution in copper but it remains in globules, which can be either small and well distributed in low-leaded bronzes, or large and irregular in highly leaded bronzes [5,6]. A factor playing a role in the formation of big lead globules in high-leaded bronzes is the cooling rate: if it is slower the cast stays fluid and lead is rejected by the freezing edge, thus forming lead globules of considerable dimensions [7].

Beside lead inclusions, another peculiar feature characterizing Chinese bronzes that is commonly reported in the literature is the presence of unalloyed copper inclusions (UCI) [8–10]. Different explanations were reported to justify their presence within archaeological bronzes. It is generally believed that a destannification process might be responsible for their formation, when they pseudormorphically replace other phases, typically the (α + δ) eutectoid. However, UCI are often reported also as spherical inclusions, thus resembling lead globules. For this reason, some researchers advanced the hypothesis that redeposition of copper might be an intermediate step of lead globules' corrosion: it has been proposed that copper is redeposited in spaces left from lead oxidation and consequent dissolution [6,9,11].

Concerning the lead globules corrosion, only a few scientific works are available. Moreover, the published articles do not provide theories for mechanisms of alteration, unless attempts to interpret the observed corrosion patterns, providing a phenomenological explanations [5,6,11,12].

As early as in 1969, Gettens proposes that lead globules are converted into cerussite ($PbCO_3$) and replaced by cuprite as an initial step of corrosion [6]. More recently, the same mechanism is proposed by McCann, whom hypothesis is that lead corrodes first, forming soluble species which migrate outwards [12]. If required condition occurs (diffusion of oxygen and migration of water from the environment), copper from the surrounding alloy dissolve forming Cu(I) species, which migrate inwards the spaces formerly occupied by lead to precipitate as cuprite.

Smith states that "in the early stages of corrosion, the copper formed by the continuing electrolytic action between it and the alloy (which serves as anode) will be deposited in any available space, such as cracks or in spaces left by the still earlier corrosion of lead. In the course of time, this copper will corrode to cuprite, which is then a pseudomorph of a lead drop that originally existed" [11].

An opposite pathway is proposed by Chase, who states that lead is replaced by cuprite, which is then reduced to metallic copper [5].

These considerations demonstrate that there is still an open debate on these issues and it is important to provide further empirical observation to validate and prove existing hypothesis and to reject others.

Empirical observations and development of phenomenological theories, relying on a large number of archaeological samples, represent the best approach to the problem, which could lead to the formulation of theories on degradation pathways [13]. Moreover, long-term processes are hardly reproducible in laboratory experiments [9].

Therefore, it is the authors' opinion, that an effective way to prove and validate hypothesis is to analyse archaeological samples exhibiting intermediate steps of degradation.

In order to provide a background and to have an overview of case studies available in the literature concerning peculiar behaviour of Chinese bronzes, a list of examples is presented in Table 1.

In particular, it was found mostly interesting the work by McCann where lead and cuprite inclusions were successfully characterized coupling elemental and molecular techniques, using

a scanning electron microscope and a μ-Raman spectrometer [12].

The present work provides the opportunity to investigate the corrosion behaviour of high-leaded bronze, typically manufactured in ancient China during the Zhou dynasty. Particular attention will be paid to the analysis of corrosion patterns in order to identify the mechanisms leading to the complex structures, especially focusing on the effect of the high amount of lead present in the alloy.

Analytical studies on archaeological bronzes, besides providing interesting insight about ancient cultures that lived thousands years ago, are often required for authentication studies. Indeed, corrosion patterns formed within thousand years of burial cannot be reproduced artificially (i.e. in depth intergranular corrosion or complex stratification of corrosion products) [14]. Moreover, long-term corrosion mechanisms occurring in natural environments represent a basic interest in corrosion science, which is only achievable through studies performed on archaeological samples.

Taking into account these statements, the authors aim at presenting a comprehensive micro-chemical study employing elemental and molecular analytical techniques. The overall scope of the study is to propose a pathway for the degradation of lead globules, examining the results obtained for the whole collection of bronze artefacts and taking into account the available literature.

3. Experimental

3.1. Materials

The present study concerns relics found in ancient burial pits in the Liangdai village, Shaanxi Province, an inland province along the middle reaches of the Yellow River, Northwest China, neighbouring with Shanxi and Henan provinces. The site was hailed as among the greatest Chinese archaeological findings of 2005, when a collaborative archaeological team, consisting of the Shaanxi Provincial Institute of Archaeology, the Weinan Municipal Institute of Archaeology and Preservation of Cultural Heritage, and the Hancheng Municipal Bureau of Heritage and Tourism, carried out the excavation of the Liangdai Cemetery Site [16,17].

The site comprises 103 tombs and 17 chariot pits: bronze horse chariots were also discovered, thus demonstrating that the tombs owned to a royal family.

The examined bronze objects were excavated from the Tomb 27. Decorative elements of a bronze chariot as well as harnesses and bells (Fig. 1) were sampled: a total of 11 fragments were withdrawn (Table 2).

The small samples, approximately 6–10 mm^2, were cold-mounted using a polyester resin (hardener and resin Serifix, Struers, Denmark, http://www.struers.com/) and cross-sectioned following the standard procedure [18,19]. Cross sections (labelled LB – Liangdai Bronzes) were polished by means of diamond pastes (6 to 1 μm) on polishing cloths.

Table 2
List of horse and chariot objects excavated from Tomb 27 in Liangdai archaeological site of Hancheng City, Shaanxi Province (Zhou Dynasty [1046 BC-221 BC]).

No.	Name	Excavation no.	Label
1	Belt Button (buckle)	M27:1089-8	LB1
2	Bronze bell	M27:24	LB2
3	Bronze bell	M27:32	LB3
4	Small tinkling bell	M27:530b	LB4
5	Small tinkling bell	M27:530a	LB5
6	Y-shape object	M27-901	LB6
7	Chariot railing	M27-967	LB7
8	Linchpin	M27-824	LB8
9	The end of the Horse bit	M27-28	LB9
10	Bronze tube with net decoration	M27:1053	LB10
11	Crisscross object	M27-1069	LB11

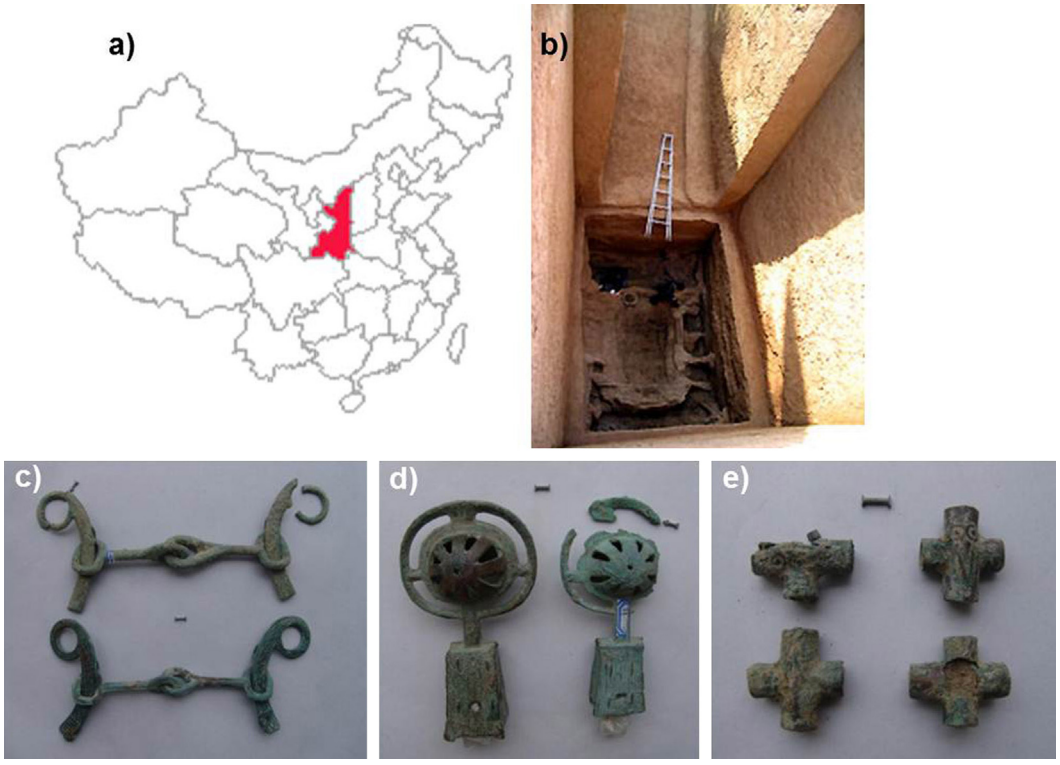

Fig. 1. Location of the Shaanxi Province in China (a) and the tomb M27 (b) where samples were discovered.

3.2. Methodologies

Metallographic sections were examined by optical microscopy in order to determine the microstructure, before and after chemical etching with solution consisting of 5% $FeCl_3$ in ethylic alcohol (98 mL) and hydrochloric acid (2 mL).

Analyses were conducted on CS by optical microscopy (OM), scanning electron microscopy coupled with energy-dispersive X-ray analysis (SEM-EDX) and μRaman spectroscopy in order to characterize the alloy compositions and microstructures, and the corrosion products generated in the burial environment.

3.2.1. Optical microscope

Samples' cross-sections were primarily examined under optical microscopy in order to document the stratigraphic morphology and colours of the corrosion layers. An Olympus (Olympus Optical, Tokyo, Japan, http://www.microscopy.olympus.eu/microscopes/) BX51 microscope fitted with a digital scanner camera Olympus DP70 equipped with fixed oculars of 10 × and objectives of 5, 10, 20, 50 and 100 × magnification were employed.

Both dark field and bright field observation were conducted, to observe respectively the corrosion products and the alloy microstructure. Microphotographs were taken using a digital scanner Olympus DX70 directly connected to the microscope.

3.2.2. Scanning electron microscope

A scanning electron microscope, Zeiss EVO 50, coupled with an energy dispersive X-ray spectrometer INCAX-sight was used on the cross-sectioned samples. The elemental composition was carried out at an acceleration voltage of 25 keV, a lifetime greater than 50 seconds and working distance of 35 mm. Semi-quantitative analysis were obtained as mean values determined on micro-areas of about 0.025 mm^2. No metallization of surface was performed.

Maps were collected over 300 seconds accumulation time. INCA software equipped with a ZAF correction procedure for bulk specimens was used for semi-quantitative analyses of X-ray intensities.

3.2.3. μRaman spectroscopy

Raman measurements were carried out in collaboration with Thermo-Scientific. A DXR Raman microscope was employed coupled to a confocal microscope with an integrated motorized stage. Objectives 10 ×, 20 × long focus and 50 × were used with laser powers ranging from 1 to 5 mW, which were chosen in order to avoid thermal degradation of the materials investigated. The spectra were collected using a 532 nm laser radiation from Nd:YAG solid state source.

The excitation source resolution, in the range 2000–50 cm^{-1}, was approximately 1.9 cm^{-1} (grating 900 lines/mm). Number of acquisition and exposure time were automatically determined by the Omnic software in order to achieve a S/N ratio higher than 100.

Under the microscope the cross-sections could be clearly seen and the area of their definite spectra could be precisely determined. Moreover, micro-Raman mapping analysis on areas of few squared microns could be performed by means of a motorized stage.

4. Results and discussion

4.1. Alloy composition and microstructure

The results obtained by optical microscope observation and SEM-EDX analysis are comprehensively presented in Table 3: the samples were grouped on the basis of the objects' typology from which they were withdrawn.

The characterisation of the alloy was, in some cases, a difficult task to achieve as many samples were deeply corroded, with few remaining uncorroded areas. Therefore the alloy composition data had to be interpreted accordingly. For the most well-preserved metal samples it was possible to evaluate the composition by SEM-EDX. Variable and very high tin (12–22 wt.%) and lead (2–15 wt.%) contents of the bronzes are coherent with the archaeological and stylistic dating of the Western Zhou period [6].

Lead was typically found as evenly dispersed regularly shaped inclusions, all over the bronze matrix, as it is immiscible within the copper α-phase. During solidification of melts, coring segregation of tin occurs within the copper α-phase when present at percentages higher than 10–15 wt.%, leading to the formation of (α + δ) eutectoid among the α-phase branches. Such behaviour was observed for all the samples.

Even in the case of completely corroded samples (LB7, LB8), some microstructural features may be deduced from the so called ghost microstructures, i.e. pseudomorphic replacement of the original alloy by corrosion products.

From a microstructural point of view all samples presented the usual α + δ eutectoid with delta fringe and presence of lead. Nonetheless, three categories could be identified:

- cored dendritic structures with lead and cuprite (Cu_2O) globules (LB1, LB3, LB6, LB7, LB9) (Fig. 2a). The dimension of inclusions is rather big, ranging from tenths to hundreds of microns. Moreover, it seems that lead inclusions are partially corroded: this is a specific and peculiar feature that deserves more attention as uncommon corrosion mechanisms are involved and further discussion will be undertaken later on;
- pure dendritic structure (LB4, LB5, LB8, LB10) with coring, being the highest concentration of tin in the delta fringe surrounding the alpha-delta eutectoid (Fig. 2b). In these samples lead is more uniformly distributed into the alloy, being mainly at dendrites boundaries. In sample LB10 this is probably due to a lower Pb content, and in the other samples to a higher cooling rate of the melt;
- a recrystallized grain structure was observed only for sample LB11 (Fig. 2c). The presence of a granular pattern and the absence of dendritic structure show that a thermal treatment has been performed after the cooling of the bronze melt.

Dendritic structures, typical for as-cast objects, were detected for most samples, thus demonstrating that objects did not undergo hammering or annealing processes. This is a typical feature of Chinese casting tradition, which is based on the piece-mould process according to which surface decoration could be made by carving it into the mould or into the model. Indeed, bronze technology reached a peak around 770 to 476 B.C. when it was usual to combine a specialized metal casting method called the lost wax technique with the piece-mould process [15].

It was not easy to justify the recrystallized structure observed for sample LB11, but an hypothesis could be that the stresses applied during the use may had the effect of modifying the microstructure, which is reasonable if one thinks at the original function of the object: a tube used to cover and strengthen the yoke [20].

4.2. Characterization of corroded patterns

Table 3 presents the corrosion patterns which were determined through optical microscope observation, both using dark and bright field illumination, together with the alloy composition and microstructures. EDX mapping was employed, thus obtaining elemental distribution at the interface alloy-corrosion layers: copper, tin and lead from the alloy, oxygen, silicon from the environment.

Most samples show a dendritic structure where the tin-rich δ-phase segregates giving rise to the formation of the α + δ eutectoid; corrosion occur by preferential removal (i.e. oxidation) of one of the phases. Selective removal depends on local environmental

Table 3
List of specimen and results obtained by scanning electron and optical microscope observation (SEM-EDX + OM).

Sample		EDX (wt. %)			Microstructure	Mean dendrites dimension	Inclusions	Corrosion
		Cu	Sn	Pb				
Harness elements								
LB1	Buckle	75 ± 2	13.6 ± 0.5	11 ± 2	Dendritic + eutectoid α+δ	n.a.	Pb (sound metal) and cuprite (corroded areas), variable dimensions	Uniform, δ-phase survives among corrosion layers, heavily corroded the globules
LB7	Bridle handle	Completely corroded			Dendritic	n.a.	Cuprite globules	Completely corroded
LB8	Linchpin	Completely corroded			Dendritic	n.a.	Cuprite globules	Completely corroded
LB9	Horse bit	76±3	14.0 ± 0.7	10 ± 3	Dendritic + eutectoid α+δ	n.a.	UCI[a] (Type B); Pb (in sound metal) and cuprite (corroded areas), variable dimensions	Uniform, heavily corroded the globules
Bells								
LB3	Bell	67.1 ± 0.8	22 ± 1	11 ± 2	Dendritic + eutectoid α+δ		UCI[a](Type A); Pb big dimension	–
LB4	Bell	73 ± 2	13.2 ± 0.8	14 ± 2	Dendritic + eutectoid α + δ	10-20 μm	UCI[a] (Type A) small, localized	Preferential δ-phase removal especially evident in the inner parts
LB5	Bell	72 ± 1	12.5 ± 0.2	15 ± 1	Dendritic + eutectoid α+δ	10–20 μm	–	Preferential δ-phase removal especially evident in the inner parts
Tubular objects								
LB6	Tubular object	73 ± 1	14.5 ± 0.3	12.8 ± 0.8	Dendritic + eutectoid α + δ	10–20 μm	UCI[a] (Type A); Pb, Cu (interior part, less corroded) and cuprite (external part, corroded), variable dimensions	Preferential α-phase removal in external layers, preferential δ-phase removal in the inner parts
LB10	Tubular object	76.6 ± 0.3	21.0 ± 0.2	2.4 ± 0.2	Dendritic + eutectoid α + δ	20–30 μm	–	Preferential α-phase removal, except locally where preferential δ-phase removal occurs
LB11	Tubular cross	73.3 ± 0.9	17.9 ± 0.9	9 ± 1	Recrystallized grain structure	–	Cuprite and cuprite + corroded lead	intergranular corrosion

[a] According to Bosi et al., 2002

condition (E-pH or Pourbaix diagrams) which changing over time lead to the idea of *corrosion trajectories* [21]. Concerning sample LB10, it is clear that the corrosion has interested only the α-phase, leaving behind the α+δ eutectoid.

It is widely reported in the literature that tin distribution allows to identify and locate the *original surface* of the object [22]. It is deduced, from E-pH diagrams, that Sn stabilizes as tin oxide (cassiterite, SnO_2) which is stable over a wide range of pH and pseudomorphically replaces the original alloy forming a passivation layer [13].

4.3. Lead globules and unalloyed copper inclusions (UCI): corrosion behaviour

As above-mentioned, a peculiar and most interesting feature of Chinese bronzes is the presence of inclusion within the bronze

Table 4
Description and characterization of the typologies of inclusions identified.

Inclusion	Description	EDX	Micro-Raman	Samples where they are present
Pb 1	Interdendritic Pb, typical behaviour due to its insolubility in the α-phase	Pb	–	LB1, LB9, LB4, LB5, LB6, LB10, LB11
Pb 2	Spheric metallic lead, irregular edges (often partly mineralized)	Pb,	Litharge, lead oxides, lead nitrate	LB1, LB9, LB6
Pb 3	Completely mineralized inclusions made up of lead- and copper- based products	Pb– Pb+Cu	Cerussite, Anglesite–Cuprite	LB6
Cu 1	Irregular shape, seems to have substituted the δ-phase (destannification process)	Cu	–	LB6, LB4, LB3
Cu 2	Spheric, in some cases Pb corrosion products are present within the globule	Cu– Cu+Pb	Cuprite–Anglesite	LB6
Cup	Round-shaped inclusion of cuprite. Sometimes, contain lead corrosion products (cerussite, anglesite)	Cu,–Cu+Pb	Cuprite, Anglesite, Cerussite	LB1, LB9, LB6, LB11

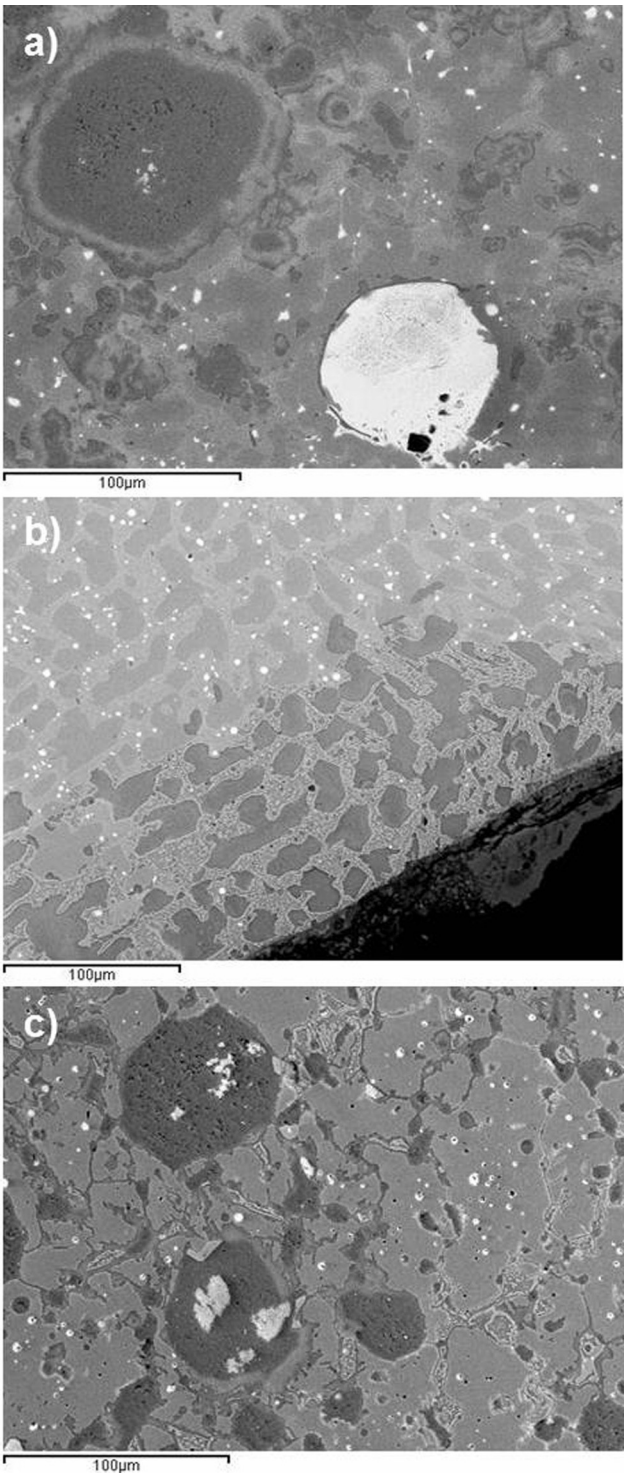

Fig. 2. BSE-SEM photomicrographs of representative microstructures: (a) cored dendritic structure (sample e.g. LB1); (b) pure dendritic structure (e.g. LB10); (c) recrystallized grain structure (e.g. LB11).

matrix. Their presence is independent from the microstructural features, as they are present also in sample LB11, which shows a recrystallized grain structure.

In the attempt to classify the inclusions, Table 4 reports an overview of the five typologies detected within all samples, together with a brief description and the samples in which they were found. They can be classified as metallic lead (labelled **Pb1**) and oxidised lead (**Pb2** and **Pb3**). A

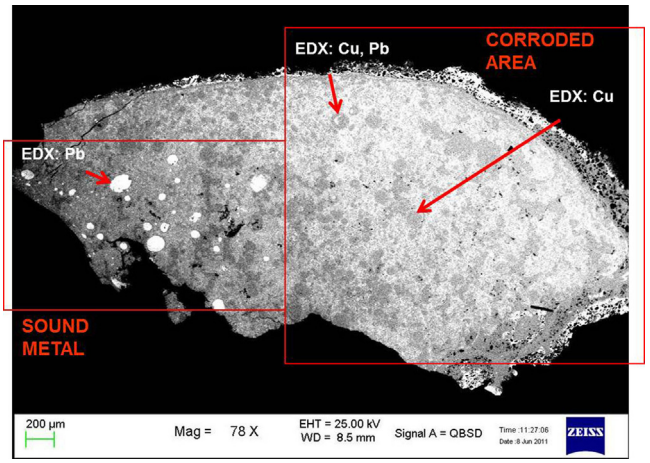

Fig. 3. BSE-SEM of sample LB9 (horse bit).

distinction is made between spherical metallic lead with irregular edges, often partly mineralized (**Pb2**), and completely mineralized inclusions made up of lead- and copper- based products (**Pb3**).

Moreover, metallic and partly corroded copper, respectively **Cu1** and **Cu2**, and cuprite (**Cup**) were found.

In particular, samples LB1 and LB9 show similar corrosion features being characterized by an extensive corrosion throughout the metallographic section. Fig. 3 shows a backscattered electron image of the metallographic section for LB9 where two regions are highlighted: the one where metal core is still preserved and the one which is completely mineralized.

In general, partially oxidized lead inclusions **Pb3** (Fig. 4a, b) were observed in the core metal, while cuprite globules **Cup** (Fig. 4c, d) are present all over the mineralized area.

Similar features are encountered in sample LB6, although this is, among the eleven fragments analysed, one of the best preserved, as sound metal core is still largely present. It might be considered to be an earlier step of corrosion, thus providing the required intermediate stage, which could help in understanding the overall degradation process.

The cross section shows the presence of the whole series of inclusions identified on the analysed samples (details of the cross section are reported in Fig. 4 e, f and 4 g, h):

- small and irregular metallic lead inclusions (***Pb1***) detected in regions where the core alloy is preserved. These represent the typical inclusions detected in leaded bronzes and are better identifiable looking at BSE-SEM images (Fig. 2);
- metallic or partly corroded lead globules (***Pb2***) localized close to metallic lead inclusion (the same type as those visible in sample LB9, Fig. 4d). Interestingly, not only lead based mineral products were found, such as lead sulphate (anglesite, $PbSO_4$) and carbonates (cerussite, $PbCO_3$), but also cuprite (Fig. 5): they are named ***Pb3***;
- a network of big cuprite globules (***Cup***) whose chemical nature was determined by μRaman spectroscopy (Fig. 5);
- a localized region of the cross section shows the presence of Unalloyed Copper Inclusion (UCI) detected within the bronze matrix both pseudomorphically replacing the eutectoid α+δ (***Cu1***) and as spherical inclusion (***Cu2***). The spherical copper inclusions are few and some of them are constituted by lead compounds, as evidenced by optical micrographs and μRaman spectroscopy (Fig. 5).

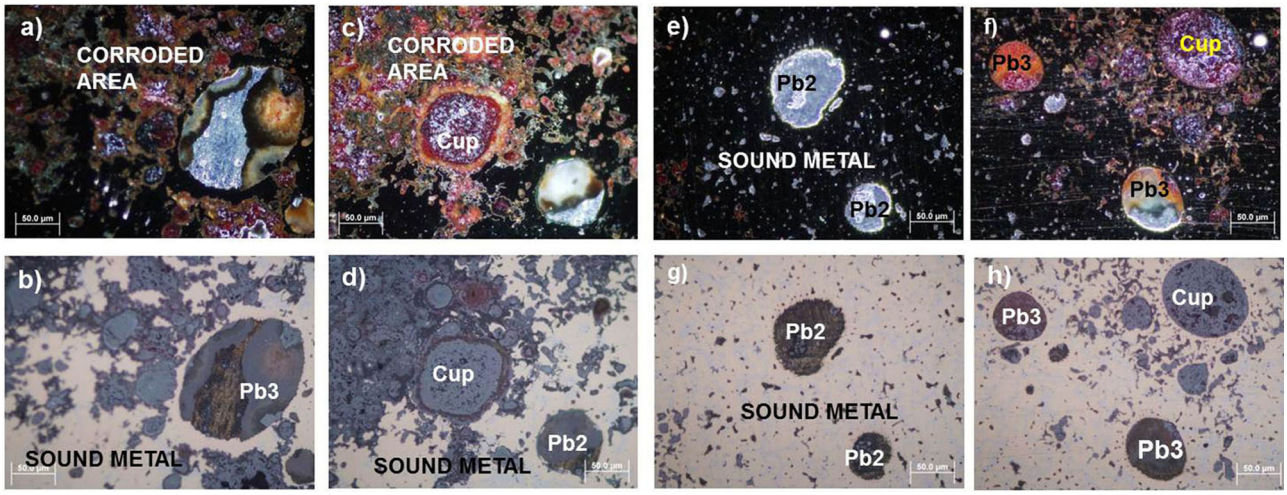

Fig. 4. Optical micrographs showing the inclusions detected in sample LB9 (a, b, c, d) and LB6 (e, f, g, h); dark and bright field illumination micrographs are reported.

A μ-Raman mapping has been performed on sample LB9 at the interface where both Pb and Cu were found (Fig. 6). Cuprite (Cu_2O, Raman band at 221 cm^{-1}) resulted to be the mineral phase present in the upper region, while lead compounds were found in the remaining area. Litharge (PbO, band at 149 cm^{-1}), lead nitrate [$Pb(NO_3)_2$ band at 1040 cm^{-1}] and lead oxide (PbO_2, band at 115 cm^{-1}) were the main phases identified and mapped over the selected area. It is worth underlining that the presence of cuprite in the upper part might be the witness of an on-going corrosion process leading to the overall conversion of lead to lead corrosion products, and eventually replaced by cuprite.

It is worth saying that lead oxides are sensitive to the laser irradiation and therefore the interpretation of spectra may be complicated because a degradation product may have formed as well [23].

All samples show a quite similar chemical composition, in particular those showing the presence of lead and copper inclusions. Sample LB1, LB6 and LB9 have tin percentage ranging from 13.6 to 14.5 and lead percentage ranging from 10 to 12.8 wt.%.

Taking into account the elemental composition of the alloy and considering the as-cast technique, we should expect a microstructure showing dendrites where lead inclusions are uniformly spread all over the cross-section. If the cooling rate is sufficiently slow, micro-segregation might occur within dendrites and lead might form bigger globules as the cast stays fluid for a longer time.

This is therefore assumed to be the initial stage and the actual observations are the result of degradation processes occurring during burial.

Thanks to the collection of archaeological bronze which were taken into account, it is possible to propose a sequence or

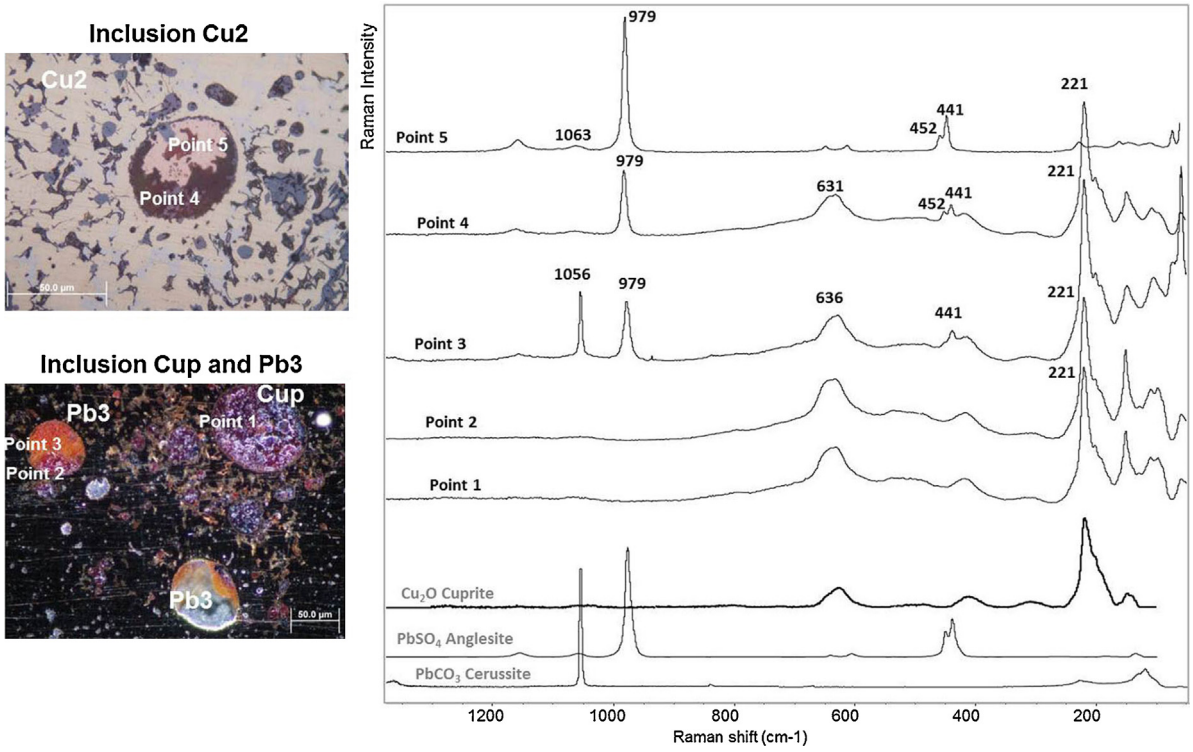

Fig. 5. Raman spectra collected within inclusions Pb3, Cu2 and Cup for sample LB6.

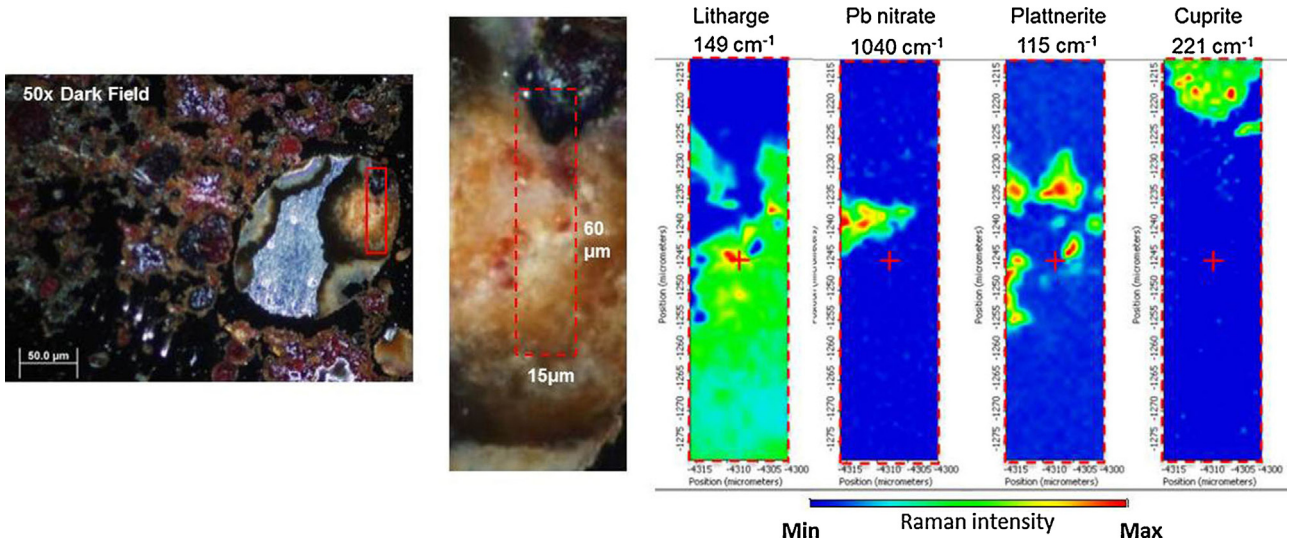

Fig. 6. µRaman chemical mapping of the partly corroded lead inclusion (Pb3) performed on the lead inclusion Pb3 identified on sample LB9.

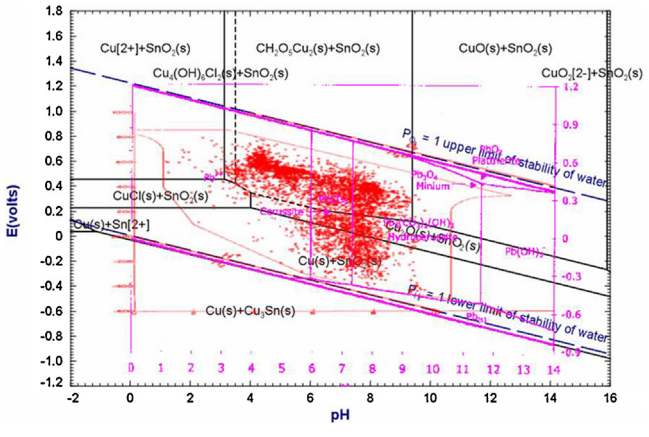

Fig. 7. E-pH diagram for the system Cu-Sn-CO_2-H_2O overlapped with Pourbaix diagram of the system Pb-CO_2-H_2O.
Extracted from presentation Pourbaix (Eh-pH or EpH). Diagrams and Archaeological corrosion of Bronzes W. Thomas Chase and Michael Notis at BUMA Beijing, Sep. 15, 2006.

mechanism for the overall transformation of lead globules into cuprite.

An hypothesis, which is supported by Pourbaix diagrams (Fig. 7) and is based on experimental observations, consists in the following sequence: metallic lead globules (**Pb2**) corrode forming oxidized lead compounds (generally named PbOX) such as oxides, sulphates and carbonates. These unstable and soluble species might, during time, diffuse and migrate outwards through porosity of the alloy and the capillary channels formed during the degradation mechanism. Within the bulk of the alloy as well as close to the surface, copper ions dissolving and corroding from the bronze alloy might oxidize (when proper condition occur) and deposit as cuprite within the voids left by the lead corrosion products. The inclusions named **Pb3**, and detected on sample LB9 and LB6, represent an intermediate stage, where lead and copper corrosion products are simultaneously present within the globules. As a final step, the original lead globule results to be completely substituted by cuprite.

The reported sequence is schematized in Fig. 8 and it can also be identified on optical micrograph of sample LB6.

The detection of metallic copper (**Cu1**) in a localized region of sample LB6 (and in LB4 as well) can be interpreted as a different phenomenon, that is ***destannification,*** taking place when values of E and pH are consistent with the stabilization of metallic copper and oxidized species of tin (SnO_2) (cfr. Fig. 7). This is explained, according to Bosi et al. as a corrosion-redeposition mechanism (in a similar manner as dezincification occurring for brass alloys) which involve a two-step process. Considering the Pourbaix diagram, it may be argued that the stabilization of metallic copper occur in reducing condition, when the dissolved oxygen is depleted due to partial anaerobic condition. Indeed, redeposited copper is present in the inner regions of the alloy, where oxygen diffusion might be more difficult (Fig. 7) [8].

It also may be argued, on the basis of experimental observations, that in these conditions, the formation of metallic copper is stabilized also within the corroded lead inclusions (Fig. 7). In fact, metallic copper together with lead corrosion products (**Cu2**) are

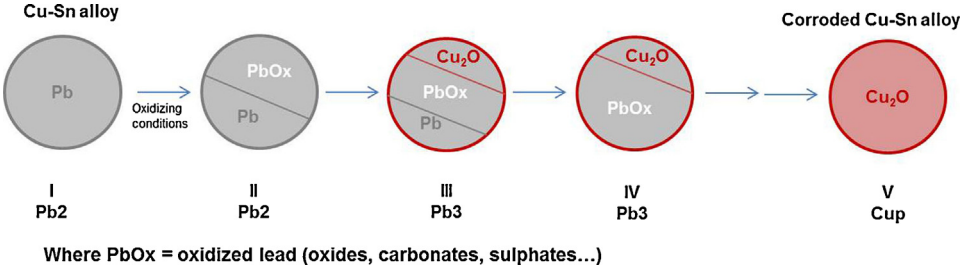

Fig. 8. A schematic sequence of the corrosion pathway of lead globules is provided.

only detected within the area of the metallographic section where UCI are present.

It is worthwhile to sum up the possible mechanisms which are involved, as they do not only involve simple electrochemical equilibria:

- thermodynamic equilibria, calculated at certain potential and pH, such as Pourbaix diagrams are invoked to determine the stable species formed (metallic Cu and Pb, lead and copper compounds) in given conditions. It is important to mention here and refer to the work by Chase et al., who determined corrosion trajectories for Cu-Sn systems on Pourbaix diagrams [21];
- kinetic of processes play an important role as these phenomena are not observed for modern bronzes and not reproducible by laboratory experiments [9]. Extremely slow reaction rates surely accounted for the occurrence of the reported mechanisms;
- solid state diffusion processes may also account for element segregation within the alloy [24].

The authors' opinion is that the subject is rather complex and difficult to be faced without possibility to be laboratory-proved. However, the analytical results obtained allowed to get an insight into behaviour of lead globules and it is relevant to have identified samples where intermediate degradation phases were detected.

5. Conclusions

On the basis of the obtained results, it may be stated that the examined archaeological bronzes offered the opportunity to investigate peculiar and complex corrosion mechanisms, which are worth to be studied in depth in order to evidence the long-term behaviour of copper alloys. Although these processes are largely investigated by several authors, this paper was focused on the poorly explored mechanism of lead globules corrosion.

The collection of archaeological samples offered the chance to identify a few of them where intermediate stages of degradation were observed.

Taking into account the experimental evidences, it could be hypothesized that the sequence leading to corrosion of lead globules consists in a direct substitution of lead corrosion products by cuprite. This could be evidenced for the first time thanks to the employed analytical techniques (a combination of elemental and molecular microscopy-based techniques) allowing a precise and detailed characterization of corroded structures. The results obtained would also help in a better understanding of empirical observation of previous studies.

Acknowledgements

We are grateful to the archaeologist Junchang Yang, from the Shaanxi Institute of Archaeology, who kindly provided the hoard of archaeological samples. We would like to kindly acknowledge Dr. Massimiliano Rocchia from Thermo Fisher S.r.l.(Milano) for the μ-Raman analysis.

References

[1] H.J. Plenderleith, A.E.A. Werner, The conservation of antiquities and works of art. Treatments, Repair and Restoration. II edition, Oxford University Press, London, 1971.
[2] D.A. Scott, Copper and bronze in art: corrosion, colorants and conservation. II ed., Getty Publications, Los Angeles, 2002.
[3] P. Northover, The complete examination of archaeological metalwork. The archaeologist and the laboratory, Council of British Council, London, 1985, pp. 56–59.
[4] W. Callister, Material Science and Engineering: an introduction, 6th Ed., Wiley International Edition, 2003.
[5] W.T. Chase, Chinese bronzes: casting, finishing, patination and corrosion, in: D.A. Scott, J. Podany, B. Considine (Eds.), Ancient, Historic Metals, The Getty Conservation Institute, London, 1994, pp. 86–117.
[6] R.J. Gettens, The freer Chinese bronzes, Oriental Studies No. 7, Technical Studies Smithsonian Institution and Freer Gallery of Art Ed, Washington DC, USA, 1969.
[7] M.J. Hughes, J.P. Northover, Problems in the analysis of leaded bronze alloys in ancient artefacts, Oxford, J. Archaeol. 3 (1) (1982) 359–364.
[8] C. Bosi, L. Garagnani, V. Imbeni, C. Martini, Unalloyed copper inclusion in ancient bronze artifacts, J. Mater. Sci. 37 (2002) 4285–4298.
[9] Q. Wang, J.F. Merkel, Studies on the redeposition of copper in Jin bronzes from Tianma-Qucun, Shanxi, China. Stud. Conservation 46 (2001) 242–250.
[10] M. Leoni, M. Diana, G. Guidi, F. Perdominici, Sul fenomeno della destannazione nei manufatti bronzei di provenienza archeologica, La Metallurgia Italiana 83 (11) (1991) 1033–1036.
[11] C.S. Smith, A search for structure., MIT Press Ed, Cambridge, Mass. USA, 1981, pp. 85–88.
[12] L.I. McCann, K. Trentleman, T. Possley, B. Golding, Corrosion of ancient chinese bronze money trees studied by raman microscopy, J. Raman Spectroscopy 30 (1999) 121–132.
[13] L. Robbiola, et al., Morphology and mechanisms of formation of natural patinas on archaeological Cu-Sn alloys, Corr. Sci. 40 (12) (1998) 2083–2111.
[14] M.L. Young, F. Casadio, J. Marvin, W.T. Chase, D.C. Dunand, An ancient Chinese bronze fragment re-examined after 50 years: contributions from modern and traditional techniques, Archaeometry 52 (6) (2010) 1015–1043.
[15] F. Bavarian, Unearthing technology's influence on the ancient Chinese dynasties through metallurgical investigations, California State University Northridge, 2005, pp. 20–26 [http://library.csun.edu/docs/bavarian.pdf].
[16] J.L. Chen, J.C. Yang, B.J. Sun, Y. Pan, Manufacture technique of bronze-iron bimetallic objects found in M27 of Liangdaicun Site, Hancheng, Shaanxi, Sci China Ser E-Tech Sci. 52 (10) (2009) 3038–3045.
[17] A Summary of a forum about the excavation of Zhou tombs at Liangdai Village in Hancheng, Shaanxi Province. Archaeol. Cultur. Relics 2 (2006) 3–6.
[18] R.N. Caron, Metallography and microstructures of copper and its alloys, Metallography and Microstructures, ASM Handbook, ASM International, 2004, pp. 775–788, ISBN: 978-0-87170-706-2.
[19] D.A. Scott, Metallography and Microstructure in Ancient and Historic Metals, Getty Conservation Institute Ed., Los Angeles, 1991, pp. 36–75.
[20] L. Liancheng, Chariot and horse burials in ancient China, The Free Library (1993) (accessed September 02 2011) http://www.thefreelibrary.com/Chariot and horse burials in ancient China-a015143740
[21] W.T. Chase, M. Notis, A.D. Pelton, New Eh-pH (Pourbaix) diagrams for the copper-tin systems, in METAL07, ICOM-CC Metal Working Group triennial conference, Amsterdam (The Netherlands), 17-21 September 2007.
[22] R. Bertholon, The original surface of corroded metallic archaeological objects: characterization and location, Rev. Metallurg. 98 (9) (2001) 817–823.
[23] L. Burgio, R.J.H. Clark, S. Firth, Raman spectroscopy as a means for the identification of plattnerite (PbO_2), of lead pigments and of their degradation products, Analyst 126 (2001) 222–227.
[24] R. Labie, W. Ruythooren, J. Van Humbeeck, Solid state diffusion in Cu-Sn and Ni-Sn diffusion couple with flip-chip scale dimension Intermetallics 15 (2006) 396–403.